Low-frequency magneto-optical excitations of a graphene monolayer: Peierls tight-binding model and gradient approximation calculation

Y. H. Chiu,[1] J. H. Ho,[1] C. P. Chang,[2] D. S. Chuu,[3,*] and M. F. Lin[1,†]
[1]*Department of Physics, National Cheng Kung University, Tainan, Taiwan 701*
[2]*Center of General Education, National Tainan University of Technology, Tainan, Taiwan 71002*
[3]*Department of Electrophysics, National Chiao Tung University, Hsinchu, Taiwan 300*
(Received 27 June 2008; revised manuscript received 23 October 2008; published 9 December 2008)

The low-frequency optical excitations of a monolayer graphene in a periodic magnetic field are calculated by the gradient approximation. The original and extra band-edge states make the optical-absorption spectra exhibit a lot of asymmetric prominent peaks, which, respectively, lead to the principal peaks and subpeaks. The two kinds of peaks obey two different selection rules because their wave functions present different features. The intensity, frequency, and number of the absorption peaks are related to the period, strength, direction of a modulated magnetic field, and the electric polarization direction. The anisotropic absorption spectra are induced by the different modulated directions and electric polarization directions. The above-mentioned results could be verified by the optical measurements.

DOI: 10.1103/PhysRevB.78.245411 PACS number(s): 78.67.−n, 81.05.Uw, 73.20.At, 75.70.Ak

I. INTRODUCTION

Recently, the few-layer graphenes have been produced by the mechanical friction[1,2] and thermal decomposition.[3,4] They have attracted a lot of theoretical and experimental investigations on band structures,[5–22] optical spectra,[5,23–29] electronic excitations,[30–33] phonon spectra,[34] and transport properties.[35–42] It is very appropriate to use these systems to study two-dimensional (2D) physical phenomena. A monolayer graphene is an exotic zero-gap semiconductor with a vanishing density of states (DOS) at the Fermi level $E_F=0$, mainly owing to the hexagonal symmetry configuration. The massless Dirac electrons have been inspected by using a combination of optical microscopy, scanning electron and atomic-force microscopies,[2] and by the angle-resolved photoelectron spectroscopy.[43] The electronic properties of a monolayer graphene could be effectively tuned by external electric[1,2] and magnetic fields.[1,2,4,5,20,22,23,25,29] A uniform perpendicular magnetic field ($\mathbf{B}_0$) creates many Landau levels (LLs) and thus induces the half-integer quantum Hall effect.[2,35] As to a periodic magnetic field, it could reveal some interesting and different physical properties, e.g., the anisotropy of low-energy electronic properties[20] and the oscillatory magnetoconductance.[44] In this work, we mainly study the low-frequency optical excitations of a monolayer graphene in a sinelike-modulated magnetic field ($\mathbf{B}$). Such a field could be produced by the array of superconducting or ferromagnetic stripes.[45,46] The dependences on $\mathbf{B}$ (period and strength; direction) and on the polarization of an electromagnetic (EM) field are investigated. The comparison with the absorption spectra resulting from $\mathbf{B}_0$ is also made.

A 2D monolayer graphene owns many doubly degenerate parabolic bands except two nondegenerate linear bands intersecting at $E_F=0$. Energy bands are isotropic at low energy ($\lesssim$0.5 eV) (Ref. 47) and so are the other physical properties.[5] Moreover, there is only one band-edge state in each energy dispersion. Electronic properties are strongly affected by the uniform and periodic magnetic fields. The low-energy LLs due to $\mathbf{B}_0$ demonstrate the dependence on the quantum number (n) and field strength (B_0); that is, their energies obey the square-root form $E_n \propto \sqrt{|n|B_0}$. The dependence on B_0 has been identified by the magneto-optical experiments of cyclotron resonance.[25] Compared to a uniform magnetic field, the periodic magnetic field could induce more rich magnetoelectronic structures.[20] The low-energy electronic structures strongly depend on a periodic magnetic field. The energy bands display partial flat bands at $E_F=0$ and parabolic bands with weak dispersions at others. Each parabolic band shows several band-edge states and composite behavior in-state degeneracy. The main features of magnetoelectronic properties are expected to be directly reflected in optical excitations.

There are several studies on optical-absorption spectra of a monolayer graphene. From the theoretical prediction, the linear valence and conduction bands do not exhibit any absorption peaks at low frequency.[5] This result is dominated by the DOS. On the other hand, the low-energy LLs in a uniform magnetic field could lead to a number of prominent symmetric absorption peaks.[5] Each peak comes from the vertical transition between the occupied LL of n ($n+1$) and the unoccupied LL of $n+1$ (n). The magneto-optical excitations need to obey the specific selection rule $|\Delta n|=1$, since the magnetoelectronic wave functions (Ψ_n's) own the spatial symmetry configuration. Ψ_n is characterized by the Hermite polynomial, as seen in a 2D electron gas. The optical selection rule has been verified by the far-infrared transmission measurements.[23] The wave functions deserve a closer investigation because they strongly affect the optical-absorption spectra. For a uniform magnetic field, the wave functions exhibit two subenvelope functions localized at two different positions in each low-energy LL except that at $E_F=0$ with only one subenvelope function. As to a modulated magnetic field, the wave functions at the original and extra band-edge states show different features. The former displays similar characteristics to those of LLs while the latter do not. The localized property of two subenvelope functions is destroyed at the latter, i.e., they overlap at the extra band-edge states. The optical-absorption spectra are expected to be modified

 ©2008 The American Physical Society

by such an overlap behavior, which implies that the optical selection rule of the spatially modulated and uniform magnetic fields might be different. The characteristics of wave functions in a modulated magnetic field will be investigated thoroughly. Whether $|\Delta n|=1$ is destroyed by a spatially modulated magnetic field will be also examined in this work.

The Peierls tight-binding model, with the nearest-neighbor atomic interactions, is used to calculate the π-electronic structure of a monolayer graphene in a spatially periodic magnetic field.[20] To explain the selection rules of optical excitations, the characteristics of magnetoelectronic wave functions are analyzed in detail. The optical transition elements are evaluated by the gradient approximation.[5,48–50] This work shows that the magneto-optical-absorption spectra present a lot of asymmetric pronounced peaks. Such peaks result from the original and extra band-edge states of parabolic bands. Their characteristics are closely related to the polarization direction and the strength, period, and direction of **B**. There exist some important differences for the absorption spectra in the presence of **B** and $\mathbf{B}_0$. The predicted results could be examined by the optical-absorption spectroscopy.

In Sec. II, the π-electronic wave functions in the presence of a spatially modulated magnetic field are studied by the Peierls tight-binding model. In Sec. III, the magnetoabsorption spectra are calculated at different polarization directions. Meanwhile, the effects due to the field strength, period, and direction are also discussed. Finally, concluding remarks are presented in Sec. IV.

II. π-ELECTRONIC WAVE FUNCTIONS

A monolayer graphene is assumed to exist in a periodic magnetic field $\mathbf{B}=B\sin(Kx)\hat{z}$ along the armchair direction [the x axis in Fig. 1(a)]. The periodic length in a unit of the lattice constant at $B=0$ $(3b')$ is $l_B=2\pi/K=3b'R_B$, where $b'=1.42$ Å is the C–C bond length. There are $2R_B$ a and $2R_B$ b atoms in a primitive unit cell. The magnetoelectronic structure formed by the $2p_z$ orbitals is described by the $4R_B$ tight-binding functions. $|a_{m\mathbf{k}}\rangle$ and $|b_{m\mathbf{k}}\rangle$ for $m=1, 2, \ldots, 2R_B$ are, respectively, those associated with the periodical a and b atoms. The π-electronic wave function is expressed as

$$|\Psi_{\mathbf{k}}^{c,v}\rangle = \sum_{m=1}^{2R_B-1} (A_o^{c,v}|a_{m\mathbf{k}}\rangle + B_o^{c,v}|b_{m\mathbf{k}}\rangle) + \sum_{m=2}^{2R_B} (A_e^{c,v}|a_{m\mathbf{k}}\rangle + B_e^{c,v}|b_{m\mathbf{k}}\rangle), \quad (1)$$

where o (e) represents an odd (even) integer. The superscripts c and v indicate the unoccupied conduction band and occupied valence band, respectively. $A_o^{c,v}$ $(B_o^{c,v})$ is the amplitude of the tight-binding function due to the a (b) atoms with odd indices. The Hamiltonian matrix in the subspace spanned by the tight-binding functions is a $4R_B\times 4R_B$ bandlike Hermitian matrix. Only the nearest-neighbor atomic hopping integrals γ_0(=2.56 eV) (Ref. 44) are taken into account. The magnetic field would induce an extra Peierls phase between two nearest-neighbor atoms at $\mathbf{R}_{m'}$ and $\mathbf{R}_m$. Such a phase is defined as $\frac{2\pi}{\Phi_0}\int_{\mathbf{R}_{m'}}^{\mathbf{R}_m}\mathbf{A}\cdot d\mathbf{r}$, where $\mathbf{A}=-B\cos(Kx)/K\hat{y}$ is the vector potential, and $\Phi_0=h/e$ is the flux quantum. To get the bandlike Hamiltonian matrix, the $4R_B$ tight-binding functions are arranged as the following sequence: $\{|a_{1\mathbf{k}}\rangle, |b_{2R_B\mathbf{k}}\rangle, |b_{1\mathbf{k}}\rangle, |a_{2R_B\mathbf{k}}\rangle, |a_{2\mathbf{k}}\rangle, |b_{2R_B-1\mathbf{k}}\rangle, |b_{2\mathbf{k}}\rangle, |a_{2R_B-1\mathbf{k}}\rangle, \ldots |a_{R_B-1\mathbf{k}}\rangle, |b_{R_B+2\mathbf{k}}\rangle, |b_{R_B-1\mathbf{k}}\rangle, |a_{R_B+2\mathbf{k}}\rangle, |a_{R_B\mathbf{k}}\rangle, |b_{R_B+1\mathbf{k}}\rangle, |b_{R_B\mathbf{k}}\rangle, |a_{R_B+1\mathbf{k}}\rangle\}$. By the detailed calculations, the nonvanishing Hamiltonian matrix elements are

$$\langle b_{m'\mathbf{k}}|H_{\mathbf{B}}|a_{m\mathbf{k}}\rangle = [t_{1\mathbf{k}}(m) + t_{2\mathbf{k}}(m)]\delta_{m',m} + t_{3\mathbf{k}}\delta_{m',m-1}. \quad (2)$$

The three hopping integrals are, respectively,

$$t_{1\mathbf{k}}(m) = \gamma_0 \exp[(ik_x b'/2 + ik_y\sqrt{3}b'/2) + G_m],$$

$$t_{2\mathbf{k}}(m) = \gamma_0 \exp[(ik_x b'/2 - ik_y\sqrt{3}b'/2) - G_m],$$

and

$$t_{3\mathbf{k}} = \gamma_0 \exp(-ik_x b')$$

$$[G_m = -i[6(R_B)^2\Phi/\pi]\cos[\pi(m-5/6)/R_B]\sin(\pi/6R_B)].$$

The similar equations could be obtained for the periodic magnetic field along the zigzag direction.

The energy dispersions $E^{c,v}(\mathbf{k},\tilde{n})$'s are obtained by diagonalizing the Hamiltonian, where $\tilde{n}$ represents the subband

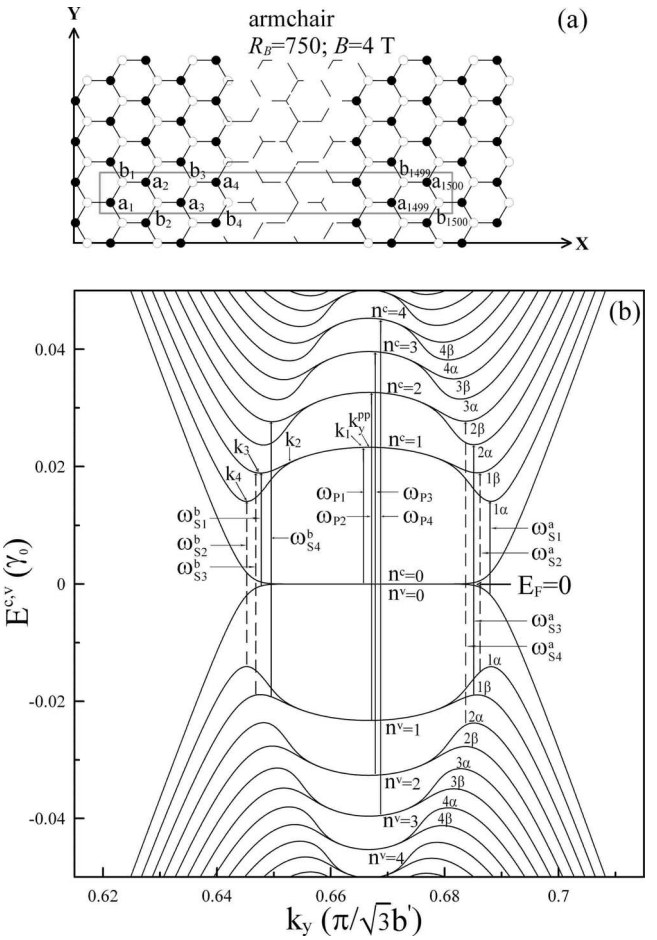

FIG. 1. (a) The primitive unit cell of a monolayer graphene in a periodic magnetic field with a period R_B=750 along the armchair direction. (b) The energy bands for the field strength B=4 T.

index measured from the Fermi level. The effects of a modulated magnetic field on the low-frequency electronic and optical properties will decrease as the energy increases. Thus the discussion focuses on the lower-energy regime. The low-energy bands are drastically changed by the modulated magnetic field, as shown in Fig. 1(b) at $R_B=750$ and $B=4$ T along the armchair direction. The unoccupied conduction bands are symmetric to the occupied valence bands about $E_F=0$. The dependence of energy bands on k_x is negligible compared with that on k_y. The k_y-dependent energy bands exhibit partial flat bands at $E_F=0$ and parabolic bands at others. Each parabolic band owns one original band-edge state (k_y^{pp}) and four extra band-edge states (k_y^{sp}'s). The former is situated at the fixed wave vector $k_y^{pp}=2\pi/3\sqrt{3}b'$, which is the same with that in the $\mathbf{B}=0$ case.[20] However, the latter depend on the period and strength of $\mathbf{B}$. The parabolic bands close to k_y^{pp} and k_y^{sp}'s are, respectively, doubly degenerate and nondegenerate. The very weak energy dispersions near k_y^{pp} mean that a periodic magnetic field owns the ability in flocking electronic states together, which is similar to LLs resulting from a uniform magnetic field. Such energy bands could be regarded as the quasi-Landau levels (QLLs), as indicated from the characteristics of wave functions.

The main features of wave functions could be utilized to define the quantum number of QLLs. Carbon atoms with odd and even indices make equal contributions to wave functions. The tight-binding functions associated with these atoms in Eq. (1) have the opposite amplitudes; that is, $A_o^{c,v}=-A_e^{c,v}$ and $B_o^{c,v}=-B_e^{c,v}$. Only discussing the amplitudes $A_o^{c,v}$ and $B_o^{c,v}$ is appropriate in understanding the wave functions. We first see the wave function of the lowest unoccupied QLL ($\tilde{n}=1$ or $n^c=0$) at k_y^{pp}. The position-dependent A_o^c and B_o^c, as shown in Figs. 2(a) and 2(g) by the solid circles, mainly come from the $2p_z$ orbitals centered at one fourth ($x_1=a_m/2R_B=1/4$) and three fourths ($x_2=b_m/2R_B=3/4$) of a primitive unit cell, respectively. The positions x_1 and x_2 correspond to the maximum field strength. The wave function of the lowest unoccupied QLL is similar to that of the highest occupied QLL [$n^v=0$ by the open circles in Figs. 2(a) and 2(g)]. Their main difference lies in the interchange of the localization positions of $A_o^{c,v}$ and $B_o^{c,v}$. Such interchange might include the sign change in the values. The distribution width of the localization function (l_B), that is, the full width at half maximum, is comparable to the magnetic length ($\sqrt{\hbar/eB}$), e.g., $l_B\approx 200$ Å at $B=4$ T. Also note that the two LLs at $E_F=0$ due to a uniform magnetic field could display the similar characteristics.[22]

There are two important differences between the second and first (lowest) unoccupied QLLs at k_y^{pp}. The former, as shown in Figs. 2(b) and 2(h), is doubly degenerate. Moreover, it is composed of two tight-binding functions centered at x_1 and x_2. A_o^c (B_o^c) has two subenvelope functions $A_o^c(x_1)$ [$B_o^c(x_1)$] and $A_o^c(x_2)$ [$B_o^c(x_2)$] located at $x_1=1/4$ and $x_2=3/4$, respectively. The oscillatory $A_o^c(x_1)$ [$B_o^c(x_2)$] owns one zero point, while the monotonic $A_o^c(x_2)$ [$B_o^c(x_1)$] has no zero point. Their contributions to wave functions are nearly comparable. The number of zero point (n), which stands for the spatial symmetry of the carrier density, could be chosen to characterize the wave functions. The effective quantum number

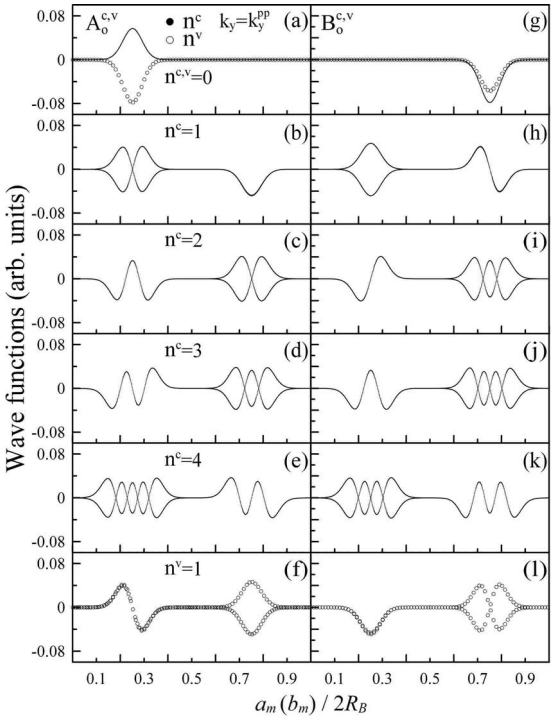

FIG. 2. The wave functions contributed by the (a)–(f) $A_o^{c,v}$ and (g)–(l) $B_o^{c,v}$ atoms with odd integer indices for original band-edge states of the low-energy bands.

(n^c) is defined by the larger number of zero point; that is, $n^c=1$ is chosen for the second unoccupied QLL. Such a choice does not influence the specific selection rules of the optical-absorption spectra. In addition, the twofold-degenerate QLLs have similar wave functions; their difference is only the sign change in the subenvelope functions. By the definition of n^c, the first unoccupied QLL without zero point is thus defined as the $n^c=0$ state. The number of zero point will become larger with the increase in state energy, i.e., n^c also increases gradually as the unoccupied QLLs are away from $E_F=0$ [Figs. 2(a)–2(e) and 2(g)–2(k)]. The $\tilde{n}$th unoccupied QLL owns two modes of subenvelope functions with $n=\tilde{n}-1$ and $n=\tilde{n}-2$, respectively. That n^c is just equal to $\tilde{n}-1$ is very convenient in defining the unoccupied QLLs [Fig. 1(b)]. Furthermore, the second occupied QLL could also reveal similar features to those in the second unoccupied QLL, as shown in Figs. 2(f) and 2(l). They have the same effective quantum number ($n^v=n^c=1$) and localization positions. Their main difference is the same as that of $n^c=0$ case. The other $\tilde{n}$th occupied and unoccupied QLLs also demonstrate the similar behavior. Accordingly, it is reasonable only to discuss the $\tilde{n}$th unoccupied QLLs.

The monolayer graphene owns many low-energy dispersionless LLs in the presence of a uniform perpendicular magnetic field. The wave functions of LLs could be represented by the linear combination of those from the harmonic oscillator.[7,46] After the well fitting, the $\tilde{n}$th QLLs and LLs show the similar characteristics, e.g., the same oscillatory behavior, effective quantum number, and distribution width. Such similarities imply that the wave functions of the former could be approximately expressed as those of the latter.

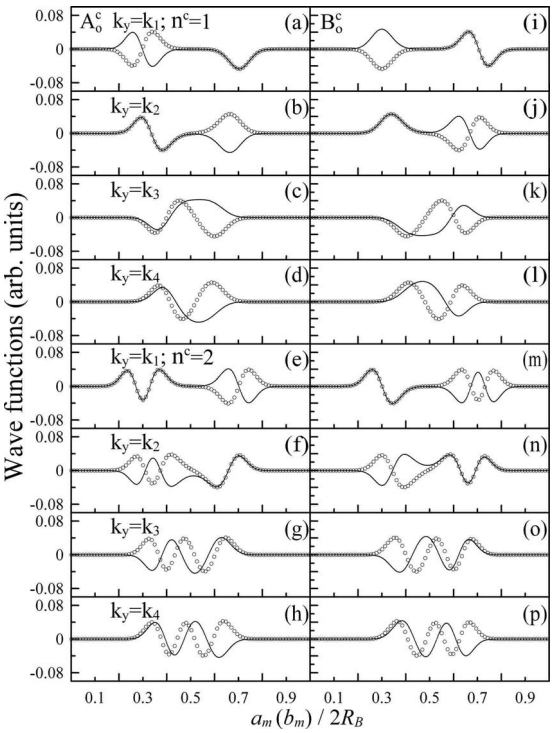

FIG. 3. Same plots as Fig. 2 but shown for the second and third conduction bands at different k_y's.

Therefore, $A_o^{c,v}$ and $B_o^{c,v}$ of the $\tilde{n}$th QLL in Eq. (1) are written as

$$A_o^{c,v} \propto e^{\pm ik_y y}\varphi_0(x_1), \quad B_o^{c,v} \propto e^{\pm ik_y y}\varphi_0(x_2) \quad \text{for} \quad \tilde{n}=1, \tag{3a}$$

$$A_o^{c,v} \propto e^{\pm ik_y y}[\varphi_{n^{c,v}}(x_1) \pm \varphi_{n^{c,v}-1}(x_2)],$$

$$B_o^{c,v} \propto e^{\pm ik_y y}[\varphi_{n^{c,v}-1}(x_1) \pm \varphi_{n^{c,v}}(x_2)] \quad \text{for} \quad \tilde{n}>1. \tag{3b}$$

The subenvelope function $\varphi_n(x)$ is the product of the nth-order Hermite polynomial and Gaussian function.[7,46]

The wave functions would be strongly modified as the wave vectors gradually move away from the original band-edge state. The wave functions at the left- and right-side wave vectors around k_y^{pp} have the similar characteristics, and thus only the former are discussed in the following part. For example, $A_o^c(x_1)$ $[B_o^c(x_1)]$ and $A_o^c(x_2)$ $[B_o^c(x_2)]$ of the second unoccupied QLL at k_1 [indicated in Fig. 1(b)] are centered at, respectively, $x_1=3/10$ and $x_2=7/10$, as shown in Figs. 3(a) and 3(i). They still maintain the same characteristics with those at k_y^{pp}, while the distance between them ($|x_1-x_2|=2/5$) is shorter than that ($|x_1-x_2|=1/2$) at k_y^{pp}. At $k_y=k_2$, the doubly degenerate QLL is going to separate into two subbands. $x_1\approx 7/20$ and $x_2\approx 13/20$ are so close that $A_o^c(x_1)$ $[B_o^c(x_1)]$ and $A_o^c(x_2)$ $[B_o^c(x_2)]$ nearly overlap, as shown in Figs. 3(b) and 3(j). Besides, one of the tight-binding functions has the opposite sign to that at k_1, i.e., A_o^c (B_o^c) might change its sign at some appropriate wave vectors. k_3 and k_4 are, respectively, the band-edge states (k_y^{sp})'s of the higher and lower subbands. Their wave functions display the similar behavior [Figs. 3(c) and 3(k); 3(d) and 3(l)]. The second unoccupied QLL at k_3 is divided into two nondegenerate subbands, i.e., the 1α and 1β subbands. The subenvelope functions of the 1α state, as shown in Figs. 3(c) and 3(k) by the solid circles, exhibit more overlap behavior. It implies that there would be strong overlap in the subenvelope functions at k_y^{sp}'s. Such a behavior would dominate the optical excitation strength. The centered positions x_1 and x_2 are close to half of a primitive unit cell, i.e., they correspond to the nearly zero magnetic field strength. In other words, the carriers will move from the position of the maximum magnetic-field strength to that of the minimum magnetic-field strength. The 1β [the open circles in Figs. 3(c) and 3(k)] and 1α subbands have the similar overlap behavior. However, $A_o^c(x_1)$ $[B_o^c(x_1)]$ and $A_o^c(x_2)$ $[B_o^c(x_2)]$ of the former display the stronger overlap than those of the latter. It results from the fact that k_3 is the extra band-edge state of the 1β subband but not that of the 1α subband. Furthermore, the two states reveal the different linear combinations of $A_o^c(x_1)$ $[B_o^c(x_1)]$ and $A_o^c(x_2)$ $[B_o^c(x_2)]$. A_o^c (B_o^c) of the 1α and 1β states could be roughly regarded as, respectively, the combination of $\varphi_1(x_1)-\varphi_0(x_2)$ $[\varphi_0(x_1)+\varphi_1(x_2)]$ and of $\varphi_1(x_1)+\varphi_0(x_2)$ $[\varphi_0(x_1)-\varphi_1(x_2)]$; that is, they might show the different spatial symmetries. The wave functions of the extra band-edge states have dissimilar characteristics to those of the original band-edge state. Since the former exhibits the overlap behavior, the localized feature of QLLs is thoroughly destroyed at k_y^{sp}'s. Such properties would be reflected on the optical-absorption spectra. The wave functions of the 2α (2β) subband [Figs. 3(g), 3(h), 3(o), and 3(p)] also display similar features as those of the 1α (1β) subband, i.e., the similar localization positions, linear combination, and the overlap behavior of the subenvelope functions. The other $\tilde{n}$th α and β subbands also present the similar characteristics. The above-mentioned characteristics of wave functions could be utilized to investigate the selection rules of the optical-absorption spectra.

III. MAGNETO-OPTICAL-ABSORPTION SPECTRA

The main features of electronic properties can be directly manifested by the optical excitations. When a monolayer graphene is excited from the occupied valence to unoccupied conduction bands (the inter-π-band excitation) by an electromagnetic field, there are only inter-π-band excitations at zero temperature. The optical selection rules $\Delta\mathbf{k}_x=0$ and $\Delta\mathbf{k}_y=0$ due to the vertical transitions are mainly determined by the zero momentum of photon. Based on Fermi's golden rule, the optical-absorption function is given by

$$A(\omega) \propto \sum_{c,v,\tilde{n},\tilde{n}'} \int_{1\text{stBZ}} \frac{d\mathbf{k}}{(2\pi)^2} \left| \left\langle \Psi^c(\mathbf{k},\tilde{n}) \left| \frac{\hat{\mathbf{E}}\cdot\mathbf{P}}{m_e} \right| \Psi^v(\mathbf{k},\tilde{n}') \right\rangle \right|^2 \times \text{Im}\left\{ \frac{f[E^c(\mathbf{k},\tilde{n})]-f[E^v(\mathbf{k},\tilde{n}')]}{E^c(\mathbf{k},\tilde{n})-E^v(\mathbf{k},\tilde{n}')-\omega-i\Gamma} \right\}, \tag{4}$$

where $f[E(\mathbf{k},\tilde{n})]$ is the Fermi-Dirac distribution function. $\hat{\mathbf{E}}$ is the unit vector of an electric polarization. The parallel and

perpendicular polarization directions $\hat{\mathbf{E}}\|\hat{x}$ and $\hat{\mathbf{E}}\perp\hat{x}$ are taken into account. The velocity matrix element $M^{cv}=\langle\Psi^c(\mathbf{k},\tilde{n})|\hat{\mathbf{E}}\cdot\mathbf{P}/m_e|\Psi^v(\mathbf{k},\tilde{n}')\rangle$ is calculated from the gradient approximation. It is approximated by taking the gradient of the Hamiltonian matrix element versus the wave vector k_x or k_y. Similar approximations have been successful in studying the optical properties of the carbon nanotubes,[45] nanographite ribbons,[46] graphite,[5] and graphite intercalation compounds.[47] Moreover, by substituting Eq. (1) into the velocity matrix element, M^{cv} is expressed as

$$\sum_{m,m'=1}^{2R_B}[(A_o^c+A_e^c)^*\times(B_{o'}^v+B_{e'}^v)+(B_o^c+B_e^c)^*\times(A_{o'}^v+A_{e'}^v)]\nabla_k\langle a_{m\mathbf{k}}|H_B|b_{m'\mathbf{k}}\rangle. \quad (5)$$

The indices o (e) and o' (e') are, respectively, the odd (even) integers of m and m'. For convenience, the value of $(A_o^c+A_e^c)^*\times(B_{o'}^v+B_{e'}^v)+(B_o^c+B_e^c)^*\times(A_{o'}^v+A_{e'}^v)$ is represented by M_{AB}^{cv}. The absolute values of $\nabla_k\langle a_{m\mathbf{k}}|H_B|b_{m'\mathbf{k}}\rangle$ for two polarization directions are

$$M_x^{cv}=|b'\gamma_0[\cos(\sqrt{3}b'k_y/2+G_m)-1]| \text{ for } \hat{\mathbf{E}}\|\hat{x}, \quad (6a)$$

$$M_y^{cv}=|\sqrt{3}b'\gamma_0\sin(\sqrt{3}b'k_y/2+G_m)| \text{ for } \hat{\mathbf{E}}\perp\hat{x}. \quad (6b)$$

The optical properties are closely related to the number and strength of excitation channels. The joint density of states (D_J) reflects the number of excitation channels. D_J is defined by setting the velocity matrix element in Eq. (4) to one. When the optical excitations come from the band-edge states, D_J would exhibit the prominent peak structures. The low-frequency D_J at $B=0$ has no special structures. It vanishes at $\omega=0$ and linearly grows with the increasing frequency (not shown).[5] The low-energy 2D linear bands do not induce any optical-absorption peaks. D_J is strongly affected by the periodic magnetic field. Figure 4(a) shows D_J's for $R_B=750$ and different field strengths along the armchair direction. They display a lot of peak structures. The peak height is enhanced with the increase in the field strength. The peaks at $\omega=0$ mainly result from the excitation channel between the two QLLs at $E_F=0$. The other peaks are dominated by the excitation channels from the original band-edge and extra band-edge states. The similar results for different R_B's and the zigzag direction at $B=4$ T are also shown in Fig. 4(b).

The optical-absorption spectrum quite differs from the joint density of states after introducing the velocity matrix element. The low-frequency spectral functions for $R_B=750$ at different B's along the armchair direction with $\hat{\mathbf{E}}\|\hat{x}$ are shown in Fig. 5(a). The periodic magnetic field has a strong effect on the spectral function. Each $A(\omega)$ exhibits rich asymmetric peaks (in the square-root divergent form at $\Gamma\rightarrow 0$). These peaks could be further divided into the principal peaks (ω_P)'s and the subpeaks (ω_S)'s according to the optical excitations resulting from the original band-edge and extra band-edge states, respectively. As the field strength rises, the peak height and frequency of the principal peaks (subpeaks) increase, and the peak number decreases. These results mean

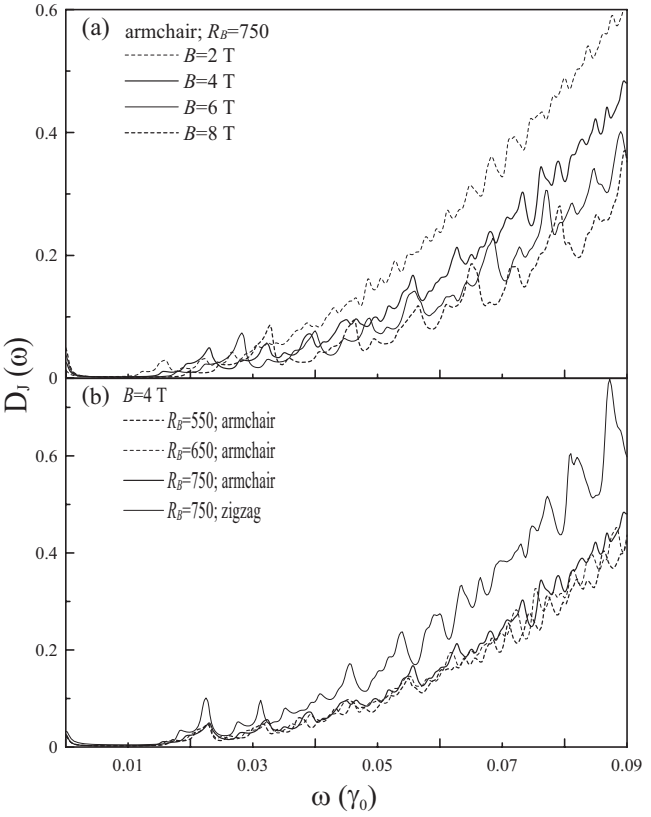

FIG. 4. The optical joint density of states for a spatially modulated magnetic field along the armchair direction at (a) $R_B=750$ and different B's; (b) $B=4$ T and different R_B's. That along the zigzag direction at $B=4$ T and $R_B=750$ is also shown in (b).

that the ability in flocking electronic states together is enhanced as the field strength grows. What is worth mentioning is that ω_S's could be further classified into two subgroups ω_S^a's and ω_S^b's because of the two kinds of subbands α and β. ω_S^a's and ω_S^b's primarily come from the excitations of α (β) to β (α) and α (β) to α (β), respectively. The peak heights of the former are very low compared with those of the latter. The zero velocity matrix elements between two QLLs at $E_F=0$ make $A(\omega)$ vanish at $\omega=0$. The optical excitation channel caused by the two QLLs is forbidden.

In addition to the field strength, the optical-absorption spectrum is also influenced by the modulated period. Figure 5(b) shows the optical spectra of $B=4$ T for different R_B's along the armchair direction. The subpeaks ω_S^a's (ω_S^b)'s strongly depend on the period, i.e., they present different peak heights and frequencies at different R_B's. Concerning the case of principal peaks, their peak heights rise with the increase in the period and their frequencies present the weak dependence on R_B. As the period grows, the electronic states tend to flock together in QLLs and some states of the nondegenerate subbands become QLLs. Moreover, the energy dispersions of QLLs near k_y^{pp} and the energy difference between two subbands near k_y^{sp}'s are reduced. The changes in energy bands could account for the dependence of optical-absorption peaks on R_B.

The low-energy optical-absorption spectra could exhibit the anisotropic feature in the presence of a modulated mag-

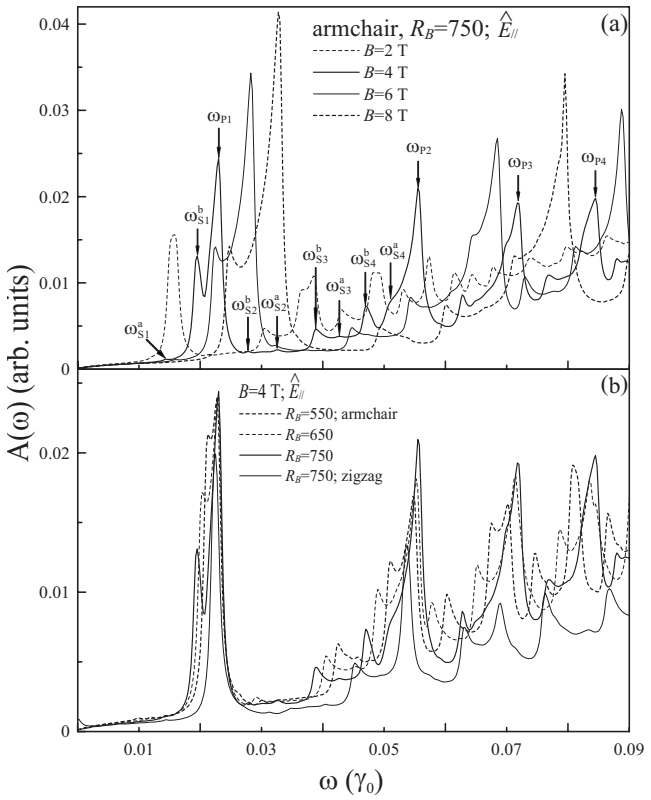

FIG. 5. The optical-absorption spectra with the electric polarization parallel to the modulated direction. They are calculated for the armchair direction at (a) R_B=750 and different B's; (b) B=4 T and different R_B's. That for the zigzag direction is also evaluated at (b) B=4 T and R_B=750.

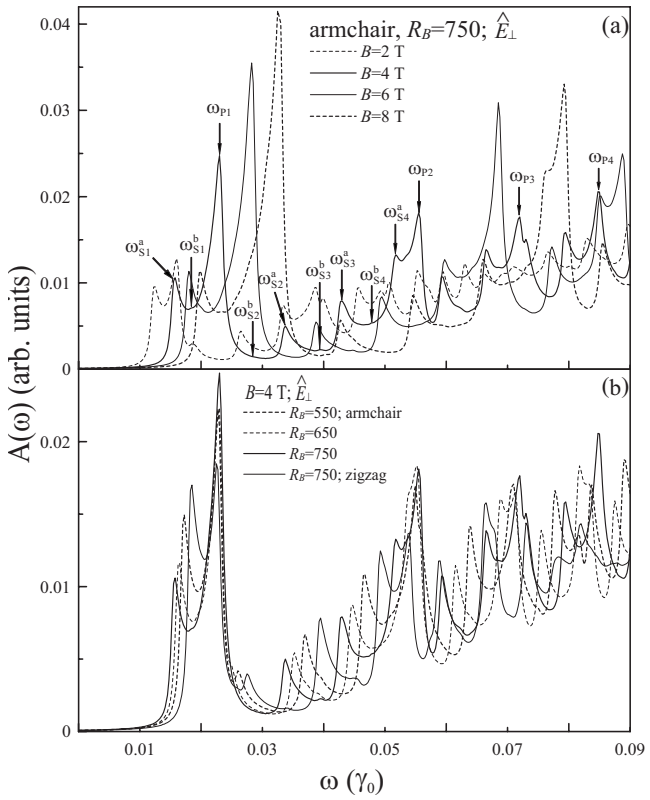

FIG. 6. Same plot as Fig. 5 but shown for the electric polarization perpendicular to the modulated direction.

netic field. $A(\omega)$ of R_B=750 at B=4 T along the zigzag direction is shown in Fig. 5(b) by the thin solid curve. ω_{P1}'s of the two modulated directions own the same energy, while the other ω_{Pn}'s do not [Fig. 5(b)]. The peak height of each principal peak from the zigzag direction is lower than that from the armchair direction. As to the subpeaks, their peak heights and frequencies are dissimilar to those from the armchair direction. The above-mentioned differences directly reflect the fact that the energy bands of the two modulated directions are anisotropic,[20] and the ability in flocking electronic states together for the armchair direction is stronger than that for the zigzag direction at the same period and field strength. These important differences imply that the low-frequency optical-absorption spectra in a modulated magnetic field could induce the anisotropic behavior. This result quite differs from those of a monolayer graphene in the absence of an external field[5] or in the presence of a uniform perpendicular magnetic field.[5]

Besides the field strength, period, and direction of a modulated magnetic field, the polarization direction of an EM wave also affects the optical-absorption spectra. $A(\omega)$'s of the perpendicular polarization direction reveal somewhat different characteristics from those of the parallel polarization direction, especially in the subpeaks. Figure 6 shows similar plots to $\hat{\mathbf{E}} \perp \hat{x}$ as those of $\hat{\mathbf{E}} \| \hat{x}$ in Fig. 5. The principal peaks which correspond to two polarization directions display similar features at the same R_B's and B's, e.g., approximately the same absorption frequency, peak height, and peak number. That is to say, ω_P's show very weak dependence on the electric polarization direction. However, the intensity of subpeaks relies strongly on the polarization direction. As to $\hat{\mathbf{E}} \perp \hat{x}$, the subpeaks of ω_S^a's are much stronger than those of ω_S^b's. The opposite is true for the $\hat{\mathbf{E}} \| \hat{x}$ case. Such an important difference might be attributed to the characteristics of the velocity matrix elements, which will be discussed in the following paragraph.

The optical excitations of each low-energy absorption peak could be clearly identified. For example, the transition channels of the first four principal peaks resulting from the original band-edge state denoted as ω_{P1}, …, and ω_{P4} in Figs. 5 and 6 are indicated in Fig. 1(b). Each prominent peak comes from two different excitation channels. The first peak ω_{P1} is mainly due to the transition from the first occupied QLL of n^v=0 to the second unoccupied QLL of n^c=1. Peaks ω_{P2}, ω_{P3}, and ω_{P4} correspond to the excitations of n^v=1 to n^c=2, n^v=2 to n^c=3, and n^v=3 to n^c=4, respectively. Because of the symmetry between the conduction and valence bands about the Fermi level, another kind of excitation channel, $n^v=n+1$ to $n^c=n$, exhibits the same optical-absorption spectrum. As a result, the selection rule could be simply represented by $|\Delta n|=|n^c-n^v|=1$. It means that the two kinds of transitions originating in QLLs, $n^v=n-1$ to $n^c=n$ and $n^v=n$ to $n^c=n-1$ at k_y^{pp}, lead to the nth principal peak with frequency ω_{Pn}.

The subpeaks originating in the extra band-edge states display more complex behavior. The excitation channels of

the first eight subpeaks (ω^a_{S1}, …, and ω^a_{S4}; ω^b_{S1}, …, and ω^b_{S4} in Figs. 5 and 6) are shown in Fig. 1(b). ω^a_S and ω^b_S could be further divided into two classes in terms of the difference between n^c and n^v. For example, the peak ω^a_{S1} is primarily due to the transition from the first occupied QLL (the occupied 1α subband) to the unoccupied 1α subband (the first unoccupied QLL) at $k_y^{sp,1\alpha}$. $k_y^{sp,n\alpha}$ ($k_y^{sp,n\beta}$) is the band-edge state of the nth α (β) subband. The peak ω^a_{S3} mainly comes from the excitations of 1α to 2β (2β to 1α) at $k_y^{sp,1\alpha}$ and $k_y^{sp,2\beta}$ and the excitations of 1β to 2α (2α to 1β) at $k_y^{sp,1\beta}$ and $k_y^{sp,2\alpha}$. The difference between n^c and n^v of ω^a_{S1} (ω^a_{S3}) is $|\Delta n|=1$, and such a difference is also observed in the principal peaks. The transitions from 1α to 1β (1β to 1α) at $k_y^{sp,1\alpha}$ and $k_y^{sp,1\beta}$ and from 2α to 2β (2β to 2α) at $k_y^{sp,2\alpha}$ and $k_y^{sp,2\beta}$ lead to, respectively, the peaks ω^a_{S2} and ω^a_{S4}. n^c and n^v of the peak ω^a_{S2} (ω^a_{S4}) own the same effective quantum number, i.e., $|\Delta n|=0$, which is very distinct from the selection rule of the principal peaks. The excitation frequencies of $n\alpha$ to $n\beta$ [$n\alpha$ to $(n+1)\beta$; $n\beta$ to $(n+1)\alpha$] are identical to those of $n\beta$ to $n\alpha$ [$(n+1)\beta$ to $n\alpha$; $(n+1)\alpha$ to $n\beta$] at the same band-edge state. This is caused by the symmetry between the conduction and valence bands about $E_F=0$. It is worth noting that in the low-energy spectra, the transition channels of $n\alpha$ to $n\beta$ at two band-edge states $k_y^{sp,n\alpha}$ and $k_y^{sp,n\beta}$ [$n\alpha$ to $(n+1)\beta$ at $k_y^{sp,n\alpha}$ and $k_y^{sp,n+1\beta}$; $n\beta$ to $(n+1)\alpha$ at $k_y^{sp,n\beta}$ and $k_y^{sp,n+1\alpha}$] have nearly the same excitation frequencies. Therefore, the peaks corresponding to these excitations are undistinguishable in Figs. 5 and 6. Furthermore, the transition channels of ω^a_S's could be divided into two classes. They are the excitations of α (β) to β (α) subbands with $|\Delta n|=1$ and $|\Delta n|=0$ except for the first peak ω^a_{S1} originating in the transition channel from the first occupied QLL (the occupied 1α subband) to the unoccupied 1α subband (the first unoccupied QLL).

ω^b_S's also present similar behavior as that of ω^a_S's. The peak ω^b_{S1} is mainly due to the transition from the first occupied QLL (the occupied 1β subband) to the unoccupied 1β subband (the first unoccupied QLL) at $k_y^{sp,1\beta}$. The excitation of 1α to 1α at $k_y^{sp,1\alpha}$ results in the peak ω^b_{S2}. The excitation energy of 1α to 2α (2α to 1α) at $k_y^{sp,1\alpha}$ almost equals that of 1α to 2α (2α to 1α) at $k_y^{sp,2\alpha}$ and of 1β to 1β at $k_y^{sp,1\beta}$. These transition channels with approximately the same energy lead to the peak ω^b_{S3}. The peak ω^b_{S4} comes from the excitations of 1β to 2β (2β to 1β) at $k_y^{sp,1\beta}$ and $k_y^{sp,2\beta}$ and from the excitations of 2α to 2α at $k_y^{sp,2\alpha}$. ω^b_S's are also simply classified into two categories. They mainly originate in the transition channels from α to α (β to β) with $|\Delta n|=1$ and $|\Delta n|=0$ except for the first peak ω^b_{S1} corresponding to the excitation of the first occupied QLL (the occupied 1β subband) to the unoccupied 1β subband (the first unoccupied QLL). The excitations of the two subgroups ω^a_S's and ω^b_S's form all transition channels with $|\Delta n|=1$ and $|\Delta n|=0$. That is to say, the selection rule of subpeaks is characterized by $|\Delta n|=1$ and $|\Delta n|=0$. Such a rule quite differs from that of principal peaks. The reason could be ascribed to the overlap behavior of wave functions at the extra band-edge states.

The velocity matrix element could govern the transition channels of the optical-absorption spectra, i.e., the selection rules might be determined by the characteristics of M^{cv}. In Eq. (5), M^{cv} is decided by the product of M^{cv}_{AB} and $\nabla_k\langle a_{m\mathbf{k}}|H_B|b_{m'\mathbf{k}}\rangle$. M^{cv}_{AB} depends on the effective quantum number not on the polarization direction. The value of $\nabla_k\langle a_{m\mathbf{k}}|H_B|b_{m'\mathbf{k}}\rangle$ [Eqs. (6a) and (6b)], on the other hand, is strongly related to the polarization direction. In the case of principal peaks, $A^{c,v}_{o,e}(x_1)$ [$A^{c,v}_{o,e}(x_2)$] and $B^{c,v}_{o,e}(x_1)$ [$B^{c,v}_{o,e}(x_2)$] of the nth QLLs own the effective quantum number $n-1$ ($n-2$) and $n-2$ ($n-1$), respectively, as shown in Fig. 2. As for the nth occupied and unoccupied QLLs, M^{cv}_{AB} is proportional to $[\varphi_{n-1}(x_1)+\varphi_{n-2}(x_2)\times\varphi^*_{n-2}(x_1)+\varphi^*_{n-1}(x_2)]$ [by the definition of Eq. (3)]. Its value vanishes because of the orthogonality of $\varphi_n(x)$. The optical excitations between the occupied and unoccupied QLLs with the same effective quantum number at k_y^{pp} are forbidden. $A^{c,v}_{o,e}(x_1)$ of the nth QLL [$A^{c,v}_{o,e}(x_2)$ of the $(n+1)$th QLL] and $B^{c,v}_{o,e}(x_1)$ of the $(n+1)$th QLL [$B^{c,v}_{o,e}(x_2)$ of the nth QLL] exhibit the same effective quantum number. M^{cv}_{AB} has a finite value between the nth occupied and $(n+1)$th [$(n-1)$th] unoccupied QLLs. In addition, by the numerical analysis, the absolute values of $\nabla_k\langle a_{m\mathbf{k}}|H_B|b_{m'\mathbf{k}}\rangle$ at k_y^{pp} for two polarization directions are almost equal. It indicates that the principal peaks of $\hat{\mathbf{E}}\perp\hat{x}$ and $\hat{\mathbf{E}}\parallel\hat{x}$ have nearly the same peak height under $|\Delta n|=1$. Concerning other $|\Delta n|$ cases, all the values of M^{cv} for both polarization directions disappeared due to the orthogonality of $\varphi_n(x)$. The selection rule is thus simply expressed as $|\Delta n|=1$. This consequence is same as that of the LLs originating in a uniform perpendicular magnetic field.[7,23,25] That the main features of wave functions at k_y^{pp} resemble those of $\mathbf{B}_0$ is the most important reason. However, there are certain important differences between QLLs and LLs. The former shows the asymmetric square-root peaks resulting from the one-dimensional (1D) parabolic bands, while the latter owns the symmetric delta-function-like peaks originating in the zero-dimensional (0D) LLs. The peak height of QLLs is lower than that of LLs. The fact that the ability in flocking electronic states together with a uniform magnetic field is stronger than that with a modulated magnetic field is the reason. As the modulated period becomes sufficiently large, the peak frequency of QLLs is weakly dependent on the modulated period. Furthermore, the low-frequency optical-absorption spectra of QLLs could reveal the anisotropic features in the different modulated directions.

The velocity matrix elements at extra band-edge states display different characteristics from those at k_y^{pp} based on the overlap behavior of wave functions. At k_y^{sp}'s, $A^{c,v}_{o,e}(x_1)$ [$B^{c,v}_{o,e}(x_1)$] and $A^{c,v}_{o,e}(x_2)$ [$B^{c,v}_{o,e}(x_2)$] have the partial overlap (Fig. 3). $A^{c,v}_{o,e}(x_1)$ [$A^{c,v}_{o,e}(x_2)$] and $B^{c,v}_{o,e}(x_1)$ [$B^{c,v}_{o,e}(x_2)$] of the nth QLLs own the effective quantum number $n-1$ ($n-2$) and $n-2$ ($n-1$), respectively. M^{cv}_{AB} of $|\Delta n|=0$ does not disappear because of $\varphi_{n-1}(x_1)\times\varphi^*_{n-1}(x_2)\neq 0$ and $\varphi_{n-2}(x_1)\times\varphi^*_{n-2}(x_2)\neq 0$. Thus the optical-absorption spectra present the subpeaks with $|\Delta n|=0$. Obviously, such peaks are mainly owing to the overlap behavior of wave functions at extra band-edge states. M^{cv}_{AB} also has a finite value for $|\Delta n|=1$ while it vanishes in the $|\Delta n|\neq 0$ and $|\Delta n|\neq 1$ cases. In addition to the value of M^{cv}_{AB} that of $\nabla_k\langle a_{m\mathbf{k}}|H_B|b_{m'\mathbf{k}}\rangle$ also dominates the subpeak intensity. It strongly depends on the polarization direction, i.e., the peak height of $\hat{\mathbf{E}}\parallel\hat{x}$ is very different from that of $\hat{\mathbf{E}}\perp\hat{x}$. Equations (6a) and (6b) are the absolute values of $\nabla_k\langle a_{m\mathbf{k}}|H_B|b_{m'\mathbf{k}}\rangle$ for $\hat{\mathbf{E}}\parallel\hat{x}$ and $\hat{\mathbf{E}}\perp\hat{x}$, respectively. By the nu-

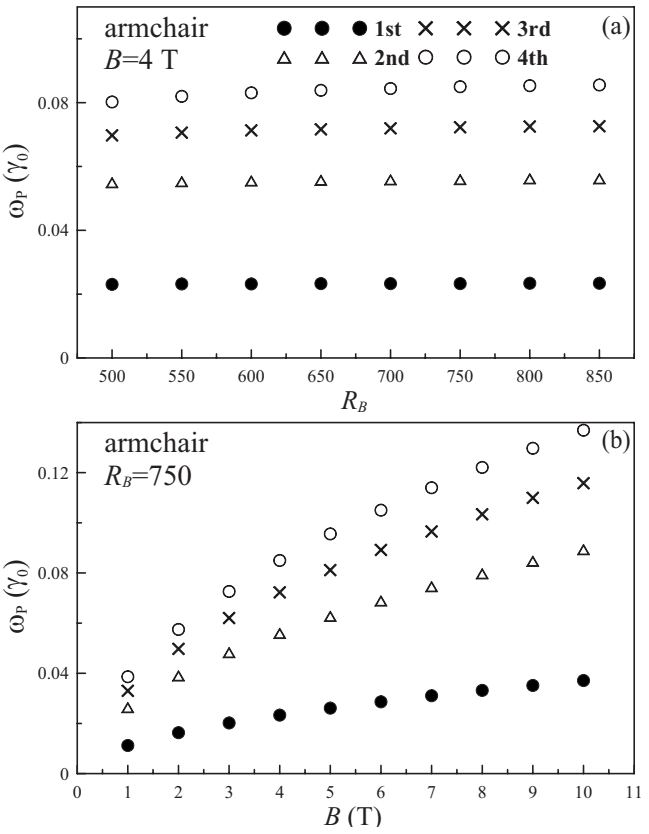

FIG. 7. The optical-absorption frequencies from the original band-edge state for a spatially modulated magnetic field along the armchair direction. Their dependences on (a) the period and (b) the field strength. The 1st, 2nd, 3rd, and 4th ω_P's correspond to the excitations of $n^v=0$ to $n^c=1$ ($n^v=1$ to $n^c=0$), $n^v=1$ to $n^c=2$ ($n^v=2$ to $n^c=1$), $n^v=2$ to $n^c=3$ ($n^v=3$ to $n^c=2$), and $n^v=3$ to $n^c=4$ ($n^v=4$ to $n^c=3$) at k_y^{pp}, respectively.

merical calculation, M_x^{cv} is much larger than M_y^{cv} ($M_y^{cv} \simeq 0$) between the occupied α (β) to unoccupied α (β) states with $|\Delta n|=0$ and $|\Delta n|=1$. However, M_x^{cv} and M_y^{cv} display the opposite behavior for the transition channels from the occupied α (β) to unoccupied β (α) states with $|\Delta n|=0$ and $|\Delta n|=1$. The difference might be ascribed to the fact that M_x^{cv} and M_y^{cv} are the sine and cosine functions, respectively. M_x^{cv}'s (M_y^{cv})'s of the excitation channels from α (β) to α (β) and from α (β) to β (α) at extra band-edge states have, respectively, the maximum (minimum) and minimum (maximum) values. That makes ω_S^a's and ω_S^b's exhibit different peak heights for two polarization directions. The subpeaks could reflect the anisotropic feature of the electric polarization direction, while the opposite is true for the principal peaks.

The frequency of principal peaks in the optical-absorption spectra deserves a closer investigation. The relation between the frequencies of the first four principal peaks and the period along the armchair direction is shown in Fig. 7(a). Energies of ω_P's present very weak dependence on the period as R_B becomes large enough. However, ω_P's strongly rely on the field strength, i.e., their energies grow with the increase in B, as shown in Fig. 7(b). It is noted that the dimension of the Hamiltonian matrix is determined by the period R_B in our calculations. It will take very long computer time in evaluating the optical-absorption spectra for the large period. Fortunately, as the modulated periods are sufficiently large, the energy dispersions and wave functions of different periods could display similar properties at a fixed field strength. That is to say, for a larger period, e.g., $R_B > 1000$, the optical-absorption spectra could be obtained by the electronic structure. As a result, the dependence on the period at the larger periods could be evaluated by observing the low-frequency energy bands, and it is the same as that at the smaller periods as shown in Fig. 7(a). As to the zigzag direction, ω_P's exhibit different frequencies from those of the armchair direction, i.e., they have the anisotropic behavior in the modulated direction. However, they display similar dependence of energies on the field strength and period (not shown in the zigzag direction). The predicted results could be verified by the optical spectroscopy.[23,25,29]

IV. SUMMARY AND CONCLUSIONS

A monolayer graphene is assumed to exist in a periodic magnetic field. The low-frequency optical-absorption spectra are studied by the Peierls tight-binding model and gradient approximation. The low-energy bands are drastically changed by the modulated magnetic field. They display the partial flat bands at $E_F=0$ and parabolic bands at others. Each parabolic band owns one original band-edge state and four extra band-edge states. Such electronic states could induce the asymmetric prominent peaks in the optical-absorption spectra. The parabolic bands close to k_y^{pp} and k_y^{sp}'s are, respectively, doubly degenerate and nondegenerate. The former could be regarded as the quasi-Landau levels based on the characteristics of wave functions. The latter are divided into two different kinds of subbands, i.e., the α and β subbands. Their wave functions display different features from those of QLLs. Wave functions deserve a closer investigation because they strongly influence the optical properties. For a uniform magnetic field, the wave functions of each LL are composed of two subenvelope functions localized at two different positions except LL at $E_F=0$ with only one subenvelope function. As to a modulated magnetic field, the wave functions show different features to those of a uniform magnetic field, and the optical-absorption spectra are modified by such differences. That is to say, the optical selection rule of a modulated magnetic field could be different from that of a uniform magnetic field. The wave functions associated with the carbon atoms a (b) of the first QLL have one tight-binding function $A_{o,e}^{c,v}(x_1)$ [$B_{o,e}^{c,v}(x_2)$] centered at x_1 (x_2). The other QLLs exhibit two tight-binding functions $A_{o,e}^{c,v}(x_1)$ [$B_{o,e}^{c,v}(x_1)$] and $A_{o,e}^{c,v}(x_2)$ [$B_{o,e}^{c,v}(x_2)$] situated at x_1 and x_2. The two positions $x_1=1/4$ and $x_2=3/4$ correspond to the maximum field strength. The wave functions of QLLs present similar characteristics to those of LLs which result from a uniform magnetic field, e.g., the same oscillatory behavior, effective quantum number, and distribution width. However, the wave functions at k_y^{sp}'s display different features. The α and β subbands own the different spatial symmetries and their two tight-binding functions exhibit overlap behavior. The different spatial symmetries and overlap behavior would induce the anisotropic features and extra excitations in the optical-absorption spectra.

The optical-absorption spectra reveal plenty of prominent asymmetric peaks. These peaks could be further divided into the principal peaks ω_P's and subpeaks ω_S's, which mainly come from the excitations of the original band-edge and extra band-edge states, respectively. The optical-absorption spectra are strongly affected by the periodic magnetic field and the polarization direction of an EM wave. The peak height of principal peaks grows as the field strength and period increase. The energy of each ω_P rises with the increase in B, and it would be weakly dependent on the period as R_B becomes large enough. As to the subpeaks, ω_S's could be classified into two subgroups ω_S^a's and ω_S^b's because of the two kinds of subbands α and β. They originate in the excitations of α (β) to β (α) and α (β) to α (β), respectively. Both of them strongly rely on the field strength and period. Furthermore, the optical-absorption spectra could reveal the anisotropic behavior in the modulated and polarization directions. The principal peaks of the armchair and zigzag directions exhibit somewhat different frequencies and the peak height of the former is higher than that of the latter. However, they display weak dependence on the polarization direction. Concerning the subpeaks, their peak heights and frequencies present strong dependence on both the modulated and polarization directions. Such anisotropy of the optical-absorption spectra could reflect the anisotropic behavior of energy bands along the two different modulated directions and the different spatial symmetries of wave functions at the extra band-edge states. ω_P's and ω_s's obey the different selection rules. The former is simply represented by $|\Delta n|=1$ and this result is the same with that of the LLs originating in a uniform perpendicular magnetic field. The most important reason is that the main features of wave functions at k_y^{pp} resemble those of $\mathbf{B}_0$. Nevertheless, the low-energy absorption spectra of QLLs and LLs still have some different characteristics. The former show the asymmetric square-root peaks because of the 1D parabolic bands, while the latter own the delta-function-like peaks due to the 0D LLs. The ability in flocking electronic states together with a uniform magnetic field is stronger than that with a modulated magnetic field, which leads to that of the peak heights of LLs being higher than those of QLLs. The peak frequency of QLLs is weakly dependent on the modulated period at sufficient large R_B's. Moreover, the low-frequency optical-absorption spectra of QLLs could exhibit the anisotropic features in the different modulated directions. As to the subpeaks, ω_s's display a different selection rule from that of principal peaks, i.e., $|\Delta n|=1$ and $|\Delta n|=0$. Such an important difference mainly comes from the overlap behavior of the wave functions at k_y^{sp}'s. The overlap behavior induces the excitations with $|\Delta n|=0$, which is forbidden in the principal peaks. Besides, the subpeaks present the anisotropy in both modulated and electric polarization directions. The selection rule and anisotropic features of optical-absorption spectra originating in a modulated magnetic field are very different from those in a uniform perpendicular magnetic field or in the absence of an external field. Such important differences could be verified by the optical measurements.

ACKNOWLEDGMENTS

This work was supported by the NSCT of Taiwan under Grants No. NSC 95-2112-M-006-028-MY3 and No. NSC 96-2112-M009-021.

*dschuu@mail.nctu.edu.tw
†mflin@mail.ncku.edu.tw

[1] K. S. Novoselov, A. K. Geim, S. V. Morozov, D. Jiang, Y. Zhang, S. V. Dubonos, I. V. Grigorieva, and A. A. Firsov, Science **306**, 666 (2004).
[2] K. S. Novoselov, A. K. Geim, S. V. Morozov, D. Jiang, M. I. Katsnelson, I. V. Grigorieva, S. V. Dubonos, and A. A. Firsov, Nature (London) **438**, 197 (2005).
[3] C. Berger, Z. M. Song, T. B. Li, X. B. Li, A. Y. Ogbazghi, R. Feng, Z. T. Dai, A. N. Marchenkov, E. H. Conrad, P. N. First, and W. A. de Heer, J. Phys. Chem. B **108**, 19912 (2004).
[4] C. Berger, Z. Song, X. Li, X. Wu, N. Brown, C. Naud, D. Mayou, T. Li, J. Hass, A. N. Marchenkov, E. H. Conrad, P. N. First, and W. A. de Heer, Science **312**, 1191 (2006).
[5] C. P. Chang, C. L. Lu, F. L. Shyu, R. B. Chen, Y. K. Fang, and M. F. Lin, Carbon **42**, 2975 (2004).
[6] S. Latil and L. Henrard, Phys. Rev. Lett. **97**, 036803 (2006).
[7] Y. Zheng and T. Ando, Phys. Rev. B **65**, 245420 (2002).
[8] E. McCann, Phys. Rev. B **74**, 161403(R) (2006).
[9] C. L. Lu, C. P. Chang, Y. C. Huang, J. M. Lu, C. C. Hwang, and M. F. Lin, J. Phys.: Condens. Matter **18**, 5849 (2006).
[10] F. Guinea, A. H. CastroNeto, and N. M. R. Peres, Phys. Rev. B **73**, 245426 (2006).
[11] E. McCann, K. Kechedzhi, V. I. Falko, H. Suzuura, T. Ando, and B. L. Altshuler, Phys. Rev. Lett. **97**, 146805 (2006).
[12] B. Partoens and F. M. Peeters, Phys. Rev. B **74**, 075404 (2006).
[13] M. Koshino and T. Ando, Phys. Rev. B **76**, 085425 (2007).
[14] C. L. Lu, C. P. Chang, J. H. Ho, C. C. Tsai, and M. F. Lin, Physica E **32**, 585 (2006).
[15] J. H. Ho, Y. H. Lai, S. J. Tsai, J. S. Hwang, C. P. Chang, and M. F. Lin, J. Phys. Soc. Jpn. **75**, 114703 (2006).
[16] E. McCann and V. I. Falko, Phys. Rev. Lett. **96**, 086805 (2006).
[17] J. M. Pereira, F. M. Peeters, and P. Vasilopoulos, Phys. Rev. B **76**, 115419 (2007).
[18] N. Nemec and G. Cuniberti, Phys. Rev. B **75**, 201404(R) (2007).
[19] J. H. Ho, Y. H. Lai, Y. H. Chiu, and M. F. Lin, Nanotechnology **19**, 035712 (2008).
[20] Y. H. Chiu, Y. H. Lai, J. H. Ho, D. S. Chuu, and M. F. Lin, Phys. Rev. B **77**, 045407 (2008).
[21] E. V. Castro, K. S. Novoselov, S. V. Morozov, N. M. R. Peres, J. M. B. Lopes dos Santos, J. Nilsson, F. Guinea, A. K. Geim, and A. H. CastroNeto, Phys. Rev. Lett. **99**, 216802 (2007).
[22] Y. H. Lai, J. H. Ho, C. P. Chang, and M. F. Lin, Phys. Rev. B **77**, 085426 (2008).
[23] M. L. Sadowski, G. Martinez, M. Potemski, C. Berger, and W. A. deHeer, Phys. Rev. Lett. **97**, 266405 (2006).
[24] D. S. L. Abergel and V. I. Falko, Phys. Rev. B **75**, 155430 (2007).

[25] R. S. Deacon, K. C. Chuang, R. J. Nicholas, K. S. Novoselov, and A. K. Geim, Phys. Rev. B **76**, 081406(R) (2007).
[26] D. S. L. Abergel, A. Russell, and Vladimir I. Fal'ko, Appl. Phys. Lett. **91**, 063125 (2007).
[27] C. L. Lu, C. P. Chang, Y. C. Huang, R. B. Chen, and M. L. Lin, Phys. Rev. B **73**, 144427 (2006).
[28] C. L. Lu, H. L. Lin, C. C. Hwang, J. Wang, C. P. Chang, and M. F. Lin, Appl. Phys. Lett. **89**, 221910 (2006).
[29] Z. Jiang, E. A. Henriksen, L. C. Tung, Y. J. Wang, M. E. Schwartz, M. Y. Han, P. Kim, and H. L. Stormer, Phys. Rev. Lett. **98**, 197403 (2007).
[30] F. L. Shyu and M. F. Lin, J. Phys. Soc. Jpn. **69**, 3781 (2000).
[31] J. H. Ho, C. P. Chang, and M. F. Lin, Phys. Lett. A **352**, 446 (2006).
[32] J. H. Ho, C. L. Lu, C. C. Hwang, C. P. Chang, and M. F. Lin, Phys. Rev. B **74**, 085406 (2006).
[33] X. F. Wang and T. Chakraborty, Phys. Rev. B **75**, 041404(R) (2007).
[34] A. H. CastroNeto and F. Guinea, Phys. Rev. B **75**, 045404 (2007).
[35] Y. Zhang, Y. W. Tan, H. L. Stormer, and P. Kim, Nature (London) **438**, 201 (2005).
[36] K. S. Novoselov, Z. Jiang, Y. Zhang, S. V. Morozov, H. L. Stormer, U. Zeitler, J. C. Maan, G. S. Boebinger, P. Kim, and A. K. Geim, Science **315**, 1379 (2007).
[37] K. S. Novoselov, E. McCann, S. V. Morozov, V. I. Fal'ko, M. I. Katsnelson, U. Zeitler, D. Jiang, F. Schedin, and A. K. Geim, Nat. Phys. **2**, 177 (2006).
[38] V. P. Gusynin and S. G. Sharapov, Phys. Rev. B **73**, 245411 (2006).
[39] V. P. Gusynin, V. A. Miransky, S. G. Sharapov, and I. A. Shovkovy, Phys. Rev. B **74**, 195429 (2006).
[40] M. Koshino and T. Ando, Phys. Rev. B **73**, 245403 (2006).
[41] J. Nilsson, A. H. CastroNeto, F. Guinea, and N. M. R. Peres, Phys. Rev. Lett. **97**, 266801 (2006).
[42] N. M. R. Peres, F. Guinea, and A. H. CastroNeto, Phys. Rev. B **73**, 125411 (2006).
[43] S. Y. Zhou, G.-H. Gweon, J. Graf, A. V. Fedorov, C. D. Spataru, R. D. Diehl, Y. Kopelevich, D.-H. Lee, Steven G. Louie, and A. Lanzara, Nat. Phys. **2**, 595 (2006).
[44] F. D. M. Haldane, Phys. Rev. Lett. **61**, 2015 (1988).
[45] H. A. Carmona, A. K. Geim, A. Nogaret, P. C. Main, T. J. Foster, M. Henini, S. P. Beaumont, and M. G. Blamire, Phys. Rev. Lett. **74**, 3009 (1995).
[46] M. Kato, A. Endo, S. Katsumoto, and Y. Iye, Phys. Rev. B **58**, 4876 (1998).
[47] P. R. Wallace, Phys. Rev. **71**, 622 (1947).
[48] M. F. Lin and Kenneth W.-K. Shung, Phys. Rev. B **50**, 17744 (1994).
[49] Y. C. Huang, M. F. Lin, and C. P. Chang, J. Appl. Phys. **103**, 073709 (2008).
[50] J. Blinowski, N. H. Hau, C. Rigaux, J. P. Vieren, R. L. Toullee, G. Furdin, A. Herold, and J. Melin, J. Phys. (Paris) **41**, 47 (1980).